New Journal of Physics
The open access journal at the forefront of physics

Deutsche Physikalische Gesellschaft DPG
IOP Institute of Physics

Published in partnership with: Deutsche Physikalische Gesellschaft and the Institute of Physics

OPEN ACCESS

RECEIVED
20 September 2021

REVISED
20 January 2022

ACCEPTED FOR PUBLICATION
26 January 2022

PUBLISHED
10 February 2022

PAPER

Few-photon storage on a second timescale by electromagnetically induced transparency in a doped solid

Marcel Hain*, Markus Stabel and Thomas Halfmann

Institut für Angewandte Physik, Technische Universität Darmstadt, Hochschulstr. 6, 64289 Darmstadt, Germany
* Author to whom any correspondence should be addressed.

E-mail: marcel.hain@physik.tu-darmstadt.de

Keywords: light storage, electromagentically induced transparency, rare-earth ion doped solid, single photon storage, long-term quantum memory

Abstract

We present the experimental demonstration of light storage towards the single photon level at a long storage time by electromagnetically induced transparency in a rare-earth ion-doped Pr^{3+}:Y_2SiO_5 crystal. We apply decoherence control by static magnetic fields and appropriately designed radio-frequency composite pulse sequences to prolong the storage time in the memory. A rare-earth ion-doped filter crystal prepared by optical pumping serves to efficiently separate the signal at the single photon level from optical noise. Multipass setups around the memory and the filter crystal improve the storage efficiency and filter selectivity. Already without decoherence control, the setup permits storage of single photons in the microsecond regime at a storage efficiency of 42%. With decoherence control we demonstrate storage of weak coherent pulses containing some 10 photons for up to 10 s at a storage efficiency of several percent. The experimental data clearly demonstrate the applicability of EIT light storage to implement a true quantum memory in Pr^{3+}:Y_2SiO_5 at long storage times. The scientific findings and technical developments are of relevance also to other protocols and media for quantum information storage.

1. Introduction

Future quantum communication technology on a worldwide scale requires quantum repeaters to overcome signal losses [1]. A quantum memory capable of storing qubits is an essential building block for such repeaters. Since photons are the most promising candidate for flying qubits, storage of photons in an efficient, long term, high fidelity and multimode memory is required for realistic implementations of quantum repeaters [2]. In recent years, impressive progress on all of these relevant criteria has been achieved. A lot of effort has been put into increasing the storage efficiency and time [3]. So far, for storage of classical light pulses the largest demonstrated storage efficiency is 92% [4] (though at a short storage time well below 1 ms) and the longest storage time is 53 min [5] (though at a very low efficiency well below 0.1%). Until then, the highest efficiency and the longest storage time of 42 s were achieved with electromagnetically induced transparency (EIT) as the storage protocol [4, 6]. For storage of single photon qubits the maximal demonstrated storage efficiency of 91% is comparable to the results achieved for classical light pulses [7]. However, the longest storage time reached so far is only 100 ms [8].

EIT is a well established tool in coherent-adiabatic light matter interaction, e.g. applied for light storage in an optical memory [9]. The basic Λ-type coupling scheme for EIT is depicted in figure 1. A strong control pulse with frequency ν_c couples an unpopulated ground state $|2\rangle$ to an excited state $|3\rangle$ (called the control transition). Coherent interaction renders the medium transparent on the probe transition $|1\rangle \leftrightarrow |3\rangle$ at frequency ν_p and also induces a strong dispersion. The latter considerably reduces the group velocity for a probe pulse (temporally overlapping with the control pulse) at frequency ν_p. The Rabi frequency on the control transition determines the group velocity. When we adiabatically reduce the Rabi frequency of the

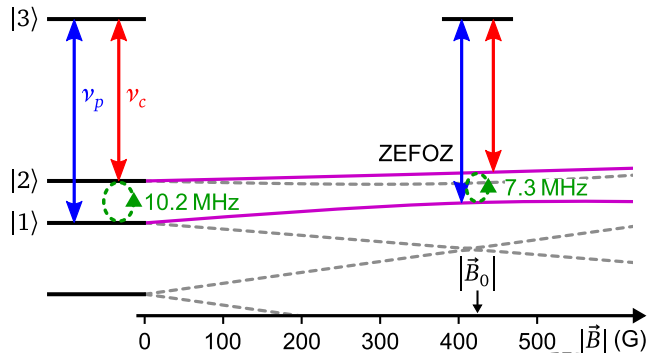

Figure 1. Schematic coupling scheme for EIT including all three $^3H_4(0)$ hyperfine ground states of Pr:YSO at zero magnetic field (left) and splitting of these states, when exposed to a static magnetic field $\vec{B}$ (dashed, gray lines on the right). ZEFOZ occurs at $\vec{B}_0$. Purple lines indicate the states applied for EIT light storage under ZEFOZ conditions.

control pulse to zero, the probe pulse is transferred into a coherent superposition of the ground states $|1\rangle$ and $|2\rangle$ (called spin transition, as typically metastable spin ground states are used). The spatio-temporal variation of the atomic coherences on the spin transition in the ensemble memory is called a spin wave. Hence, the probe pulse is stored in this spin wave by the control 'write' pulse. When we increase the control Rabi frequency again after some arbitrary storage time, this control 'read' pulse beats with the atomic coherences to retrieve a signal pulse from the memory. Under ideal conditions, the signal pulse is a copy of the input probe pulse.

Apart from EIT, there are also other protocols for photon storage [10]. Prominent examples are atomic frequency combs (AFC) [11] or controlled reversible inhomogeneous broadening (CRIB) [12, 13]. A recent approach used noiseless photon echos (NLPE) [14]. In contrast to EIT, these protocols do not employ a strong control field which coincides with the signal. However, they also require a time-delayed mapping field to transfer a short-lived optical coherence to a long-lived spin coherence. Nevertheless, as an advantage of AFC, CRIB, and NLPE there is less noise added to the signal by the delayed mapping pulse, which permits a higher storage fidelity. Furthermore, the multimode storage capacity scales more favorably with the optical depth (OD) of the memory compared to EIT [15]. On the other hand, EIT requires neither the preparation of broad absorption patterns of multiple, narrow spectral lines (as a prerequisite for AFC) nor the application of precisely controlled, large external electric fields (which is required for CRIB). Compared to NLPE, EIT requires only couplings among three atomic states and directly prepares a long-lived spin coherence—while NLPE applies four states to create a short-lived optical coherence. Mapping the latter onto a spin coherence would require even a fifth state in NLPE.

The maximum efficiency for all these storage protocols is only limited by the OD on the $|1\rangle \leftrightarrow |3\rangle$ transition and converges towards 100% with increasing OD [16]. The storage time is limited by the lifetime T_2 of the atomic coherences on the $|1\rangle \leftrightarrow |2\rangle$ transition. Hence, prolonged storage times require decoherence control, and large storage efficiencies require large OD.

In gases the storage times rarely exceeded the millisecond range—with few exceptions in trapped atoms [8, 17], Bose–Einstein condensates [18], and under very particular experimental conditions [19, 20] where a storage time of up to 16 s was achieved. For realistic applications, solid-state storage media are a more appropriate choice—as they offer scalability, easy handling and integration into quantum information architectures [10]. In particular, rare-earth ion-doped solids exhibit an atom-like level structure with long-lived ground state levels [21, 22]. Therefore, they combine the benefits of atomic media and solid-state memories. In our previous work we implemented light storage for up to 42 s in a rare-earth ion-doped Pr^{3+}:Y_2SiO_5 crystal (though at a low storage efficiency below 1%) [6], as well as efficient EIT storage reaching 76% (though at a short storage time of 2 μs) [23]. In the latter work, we embedded the memory crystal in a rather simple multipass setup to increase the effective OD. Alternative (though technically more challenging) approaches use cavities for the same purpose [24–29]. Sufficiently large storage efficiency is a crucial prerequisite to store single photons, in particular at longer storage times. However, there are yet no successful experiments of light storage on the few or single photon level (no matter which protocol) beyond short storage times of at most 100 ms. In our work presented in the following we demonstrate EIT light storage of weak coherent pulses at the single and few photon level in Pr^{3+}:Y_2SiO_5, reaching storage times in the regime of seconds. We combine decoherence control techniques to prolong the coherence lifetime with multipass setups to increase the storage efficiency as well as the performance of a rare-earth ion-doped filter crystal. The latter reduces the optical noise for detection of stored light towards the single photon level.

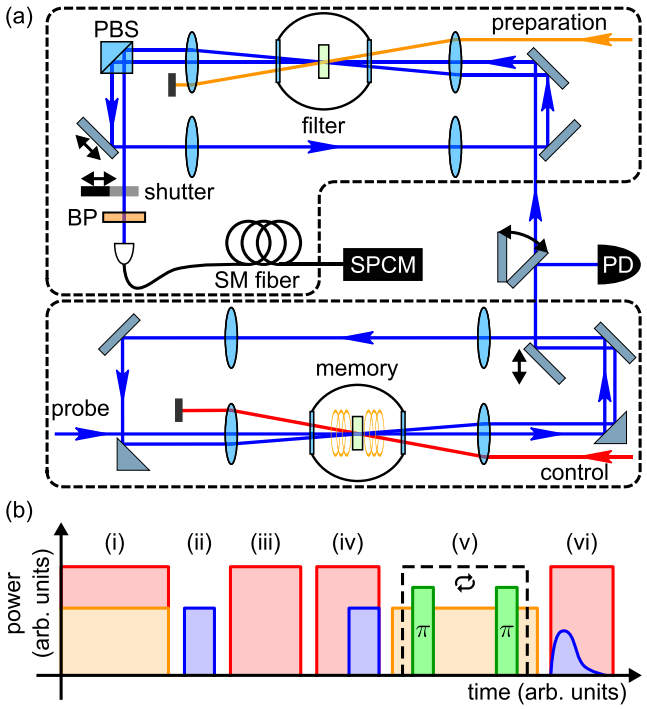

Figure 2. (a) Experimental setup involving a polarizing beamsplitter (PBS), bandpass filter (BP), single mode (SM) fiber, single photon counting module (SPCM), and a photodiode (PD). The top part shows the spectral filter section and the bottom part the memory setup, each centered around a Pr:YSO crystal (green rectangles) placed in a cryostat. In both parts, the number of passes can easily be varied by translating a single mirror. (b) Time sequence of optical and RF pulses (see main text). Green represents RF pulses, other colors indicate optical beamlines.

2. Experimental setup

We implement EIT light storage among hyperfine states of the optical $^3H_4 \leftrightarrow {}^1D_2$ transition in Pr^{3+}:Y_2SiO_5 (in the following termed Pr:YSO) at a wavelength of 605.98 nm. The population lifetime of the relevant hyperfine ground states is $T_1 \approx 100$ s which limits the maximal light storage time (if we assume full control or suppression of additional decoherence processes). The excited state lifetime is $T_1 = 164\ \mu$s. The optical transition exhibits an inhomogeneous broadening of several GHz, while the hyperfine states are separated only by ~ 10 MHz. Therefore, in an unprepared medium a single frequency laser couples all possible transitions in different ions within the large inhomogeneous linewidth. Thus, we use optical preparation sequences prior to the light storage experiments to generate an appropriate absorption spectrum, i.e. a Λ-type three-level system as required for EIT. For details on the preparation sequence see [23, 30, 31]. We note, that when we apply a magnetic field to prolong the coherence time, the level system becomes much more complex (see figure 1) and we require a modified optical preparation sequence (see below).

The experimental setup involves two major sections. In the first section we implement EIT storage in a Pr:YSO memory crystal (length 3 mm, 0.05% dopant concentration). The second section with a Pr:YSO filter crystal serves to separate the retrieved signal on the few- or single photon level from optical background (see figure 2(a)). The crystals are cooled to temperatures below 4 K in continuous flow cryostats (ST-100, Janis Research Co.). Let us first consider the memory process. We choose the polarization of all optical beams along the D_2 crystal axis in order to enable maximal coupling strength, i.e. large OD. The memory crystal is placed in the center of three superconducting Helmholtz coils (not shown in figure 2(a)) which can generate static magnetic fields of up to 0.2 T in arbitrary directions to prolong the coherence time by 'zero first order Zeeman shifts' (ZEFOZ) [32]. For further extension of storage times we implement dynamical decoupling (DD) [33] using magnetic radio-frequency (RF) pulses. We generate the RF pulses by an arbitrary waveform generator (AWG 5014, Tektronix), amplify them to a maximum power of 30 W (LZY-22+, Mini-Circuits), and transmit the pulses to the memory crystal via an impedance-matched pair of Helmholtz coils. We reach a maximal Rabi frequency of $2\pi \times 12$ kHz on the RF spin transition between the hyperfine states which carry the spin wave. We discuss details on ZEFOZ and DD further below.

All laser beams for the experiment are derived from a fiber laser pumped, frequency-stabilized, optical parametric oscillator (OPO) with internal sum frequency generation. The system yields a typical optical power of up to 500 mW available for the experiment, and a typical linewidth well below 100 kHz (full width

at half maximum, FWHM). For details on the laser system see [34]. Each of the beamlines shown in figure 2(a) involves acousto-optic modulators for frequency and amplitude modulation. This enables generation of arbitrary pulse shapes in time and frequency to provide the probe pulse and the write/read control pulses for EIT light storage, as well as the preparation sequences (using the control beamline for the memory crystal).

The probe beam passes the memory crystal N times by traveling through a ring-type multipass setup with embedded relay imaging in order to increase the OD and, hence, the storage efficiency (for details see [23]). Since the latter rather simple ring geometry does not involve a cavity, there is no need for active stabilization [26, 35] nor fine tuning of mirror reflectivities and positions [27–29]. However, as the signal in the multipass setup is coherently built up from the read-out signals after each individual pass, we must maintain interferometric stability from storage to readout, i.e. over several seconds in our experiments. We achieve this by purely passive means, i.e. proper choice of optical mounts and covering the optical table with sound absorbing foam.

The beam dimensions in the memory crystal are roughly $150 \times 130\ \mu\text{m}^2$ (FWHM, width $\times$ height) for the probe beam and $620 \times 360\ \mu\text{m}^2$ (FWHM) for the control beam. The elliptical shape and larger size of the control beam ensures a similar intensity for all probe beam passes in the multipass setup over the whole crystal length. Typically, we use control pulse powers of $\sim$10 mW, corresponding to Rabi frequencies of $\sim 2\pi \times$ 100 kHz in the interaction region. To suppress optical background due to the intense control pulses, we choose the control beam path counterpropagating to the probe beam with a small angle of 1° in between.

After the retrieved signal pulse exits the multipass setup, we measure the power on a photodiode (2051-FS, New Focus) if we performed storage of classical pulses. Alternatively, we apply a single photon counting module (SPCM-780-41-FC, Excelitas Technologies), if we performed storage of weak coherent pulses. To provide probe pulses on the few photon level, we use neutral density filters in the probe beam line. We determine the pulse energy of the retrieved signal pulses, including potential background signal, by integration of the measured pulse power in time (for classical pulses), or summing up the photon counts (for weak coherent pulses). We determine the background level by either integrating over intervals with expected zero signal pulse intensity at later times (for classical pulses) or via the number of detected photons in a storage experiment without probe pulse (for weak coherent pulses). We measure the input probe pulse energy during a stage of the preparation where there is no absorption in the memory crystal. This allows us to automatically compensate for optical losses. From the background corrected signal and input probe pulse energies E_s and E_p we calculate the light storage efficiency $\eta_\text{LS} = E_\text{s}/E_\text{p}$.

In the EIT light storage protocol the generated signal pulse temporally overlaps with the intense control read pulse. The latter is the major source of optical background. This is a particular obstacle, when it comes to storage at the few photon level. Assuming a typical control pulse power of $\sim$10 mW, a signal pulse duration of $\sim$10 s and a storage efficiency of $\sim$30%, we require a suppression of the control read pulse by 120 dB in order to enable a signal-to-noise ratio (SNR) of 1 for detection of single probe photons stored in the memory. Higher suppression would be desirable, as it increases the fidelity. Since time gating cannot be used to suppress the control background and both interacting beams must exhibit the same polarization to maintain large OD in Pr:YSO, only the options of spatial and spectral filtering remain [36, 37]. Our setup with a small angle between the counterpropagating probe and control beams and a single mode fiber covering a small solid angle in front of the single photon detector leads to a control suppression of roughly 70 dB by spatial filtering.

Thus, the remaining 50 dB suppression must be achieved by spectral filtering. In our Pr:YSO memory, the frequency difference between the control and probe pulses is quite small, i.e. in the range of $\nu_\text{p} - \nu_\text{c} \approx 10$ MHz. Dispersive elements cannot reach such a high frequency resolution. A high-finesse Fabry–Perot cavity as an interferometric spectral filter might achieve the goal, but is technically challenging. Therefore, we applied a second Pr:YSO crystal (filter crystal) as a programmable bandpass filter (see figure 2(a)). We consider now this second section of our experimental setup. The idea is to prepare the broad inhomogeneous bandwidth of Pr:YSO by optical pumping such that photons at the probe frequency are transmitted in a narrow spectral hole while the control background is strongly absorbed outside the spectral hole [38, 39]. The filter crystal is 3 mm long, has a dopant concentration of 1%, and a peak optical depth of OD $\approx$ 10. This dopant concentration leads to a high inhomogeneous linewidth of $\Gamma = 280$ GHz (FWHM). In our setup, we found the large bandwidth of the sample at high concentration to be an advantage compared to a crystal at 0.05% dopant concentration and 10 mm length with $\Gamma = 15$ GHz. We attribute this advantage to the output spectrum of our OPO light source. We suspect that it exhibits a broad (though very weak) pedestal of radiation with a bandwidth in the range of a few 100 GHz. This is roughly the acceptance bandwidth of the OPO process. The very weak, spectrally broad pedestal usually plays no role compared to the orders-of-magnitude more intense emission with narrow linewidth $\leqslant$100 kHz.

However, it becomes an obstacle when we intend to filter single signal photons from the control background with a large suppression of the latter. Thus, experimentally we found a slightly improved filter performance using the 1% doped crystal compared to the sample at 0.05% concentration, although both crystals have the same peak OD.

In our filter setup we apply a third laser beamline (see orange line in figure 2(a)) for optical pumping of the filter crystal. First, we burn six spectral holes at frequencies such that the corresponding anti-holes occur at the control frequency ν_c. This increases the control absorption by up to a factor of three compared to the unprepared medium. Second, we fill the spectral holes in the frequency interval between the control and the probe frequencies ν_c and ν_p by pumping population from spectral holes at matching frequencies. This ensures absorption of broadband background between ν_c and ν_p, while creating transmission windows only where the background is assumed to be lower. Finally, we provide for maximal signal transmission by optical pumping at the probe/signal frequency ν_p. All optical pumping pulses are chirped over 800 kHz around their center frequencies to generate a broad absorption plateau at ν_c and maximize the transmission at ν_p.

To further increase the absorption of the filter crystal for the control background, we use a multipass geometry similar to the memory section. Typically, we apply a double pass through the filter crystal, as depicted in figure 2(a). Since the polarization of the transmitted portion of the suppressed light is rotated by the filter crystal [40] we replace one mirror of the multipass setup by a polarizing beamsplitter cube. This maintains a large absorption on consecutive passes through the filter crystal. A mechanical shutter blocks stray light during the filter preparation process and a bandpass filter (#65-103, Edmund Optics) with a spectral bandwidth of 10 nm (FWHM) blocks fluorescence from other transitions in either Pr:YSO crystal. Finally, a single mode fiber guides the probe photons to the SPCM for detection.

We note, that in the double pass geometry for the filter crystal the filter absorption increases as expected for two passes rather than a single pass. However, the increase in OD is only from 10 (for a single pass) to 12 (for a double pass), i.e. much less than the expected factor of two. This is due to the weak, but broadband pedestal in the spectrum of the OPO output, which leaks through the narrowband spectral pit prepared at ν_p. Since the transmission at this frequency is maximal, the light leaked through is not affected by an increasing number of roundtrips in the multipass setup. This limits the achievable control read pulse suppression. Therefore, we apply only two passes through the filter crystal. The overall transmission of the filter setup in this case is roughly 15%. In combination with a detector efficiency of 66%, we are able to detect roughly 10% of all signal photons retrieved from the memory section.

Figure 2(b) shows the time sequences in our experiment. First, we apply optical pumping sequences to prepare maximal background suppression in the filter crystal and an optical pit in the memory crystal (i). Second, we measure the probe pulse energy transmitted through the spectral pit with zero absorption as a reference (ii). Third, we prepare a Λ-system for EIT in the memory crystal by optical pumping (iii). Fourth, we perform the write step of EIT light storage, involving the control write pulse to store the probe pulse (iv). For prolonged storage times $t_s > 2\ \mu$s we apply additional rephasing RF sequences (and ZEFOZ, see below). Moreover, we refresh the preparation of the filter crystal, if t_s is longer than the optical pumping sequence (i.e. 1 s) (v). Finally, we perform the read step of EIT light storage, involving the control read pulse and retrieving the signal pulse (vi).

3. Experimental results

3.1. EIT light storage at the single photon level

In a first experiment we apply our setup in a single pass through both the memory and the filter crystal and without magnetic decoherence control technology (ZEFOZ and dynamical decoupling) to prolong the storage time. In this case the inhomogeneous broadening of the spin transition leads to a dephasing of the coherence and limits the storage time to $T_2^* \approx 10\ \mu$s. This effect could be easily compensated by simple rephasing, e.g. with two π pulses. However, in this first experiment we focus on efficient storage at the single photon level rather than any prolongation of the storage time. We perform EIT light storage for weak coherent probe pulses with a rectangular temporal profile of pulse duration 8 μs. The control Rabi frequency is $\sim 2\pi \times 185$ kHz.

We attenuate the probe pulse intensity down to the level of a single photon, i.e. to an average photon number of $\bar{n} = 1.1 \pm 0.1$. Figure 3 shows the input probe pulse (blue data) and the retrieved signal pulse (green data) for EIT light storage with a storage time of $t_s = 2\ \mu$s, measured as the time difference between the falling edge of the control write pulse and the rising edge of the control read pulse (indicated by dashed, gray lines). The short storage time is well below T_2^*. Hence, no rephasing is required.

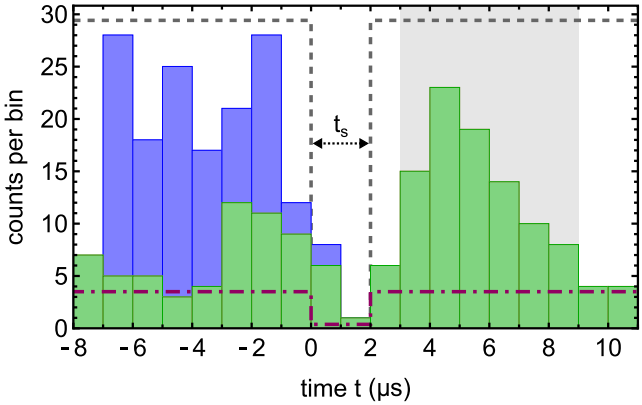

Figure 3. EIT light storage for a probe pulse with $\bar{n} = 1.1 \pm 0.1$. Photon counts (accumulated over 1000 repetitions) vs time for the probe pulse (blue) and the retrieved signal (green). The storage time is set to $t_s = 2\ \mu$s. The signal pulse shows some intensity appearing already during the write process for times $t \leqslant 0\ \mu$s. This is the fraction of the probe pulse which is not stored (due to the finite storage efficiency) and leaks through the memory. The dashed, gray line indicates the temporal shape of the control pulses and the dash-dotted, purple line shows the average noise level. The gray shaded area indicates the integration gate for the signal.

As the data in figure 3 clearly demonstrate, we detect a signal pulse very well distinguishable from the background (indicated by the dash-dotted, purple line), with an SNR of 3.2 ± 0.9. This is sufficiently large to enable operation of the storage protocol as a true quantum memory. From the data we determine a storage efficiency of $\eta_{\mathrm{LS}} = (42 \pm 7)\%$, which fits to our expectation for the measured optical depth OD ≈ 6 of the memory crystal. The uncertainties result from Poissonian statistics and could be further reduced by accumulating over more experimental cycles. Additionally, application of the multipass setup, or optimization of the temporal profile of the probe pulse [41, 42] would further improve the storage efficiency and, hence, the SNR. We apply them in our experiments towards prolonged storage times. Nevertheless, already the results in figure 3 represent, to the best of our knowledge, the first implementation of EIT light storage at the single photon level in a solid-state system.

3.2. Storage supported by ZEFOZ and multipass setup

The experiment discussed above was performed at a short storage time $t_s = 2\ \mu$s. We proceed now to significantly prolong the storage time by decoherence control techniques, while maintaining the large noise suppression for storage of few-photon pulses also at much longer time scales. In our previous work on EIT light storage of classical pulses [6], we increased the coherence decay time in Pr:YSO by ZEFOZ, induced by a strong, static magnetic field with full control of field strength and direction in three dimensions, in combination with DD, driven by RF pulses tuned to the spin transition. In short, ZEFOZ prepares appropriate nonlinear level splittings such that a magnetic transition becomes (in first order) insensitive to fluctuations of the magnetic field (see figure 1). At the same time, the applied magnetic field also reduces the rate of spin flips of yttrium ions in the crystal, which lowers the magnetic field noise in the vicinity of the praseodymium ions. The specific choice of a static magnetic field $\vec{B}_0$ in three dimensions, which provides such ZEFOZ conditions, is called a ZEFOZ point [32]. The spin wave can be further decoupled from the environment by appropriately designed sequences of RF pulses. In the simplest case, i.e. a Carr–Purcell–Meiboom–Gill (CPMG) sequence, such a DD sequence is built by repeated application of identical π pulses with a time delay which is shorter than the correlation time of the noise fluctuations in the environment [33, 43, 44].

We apply now ZEFOZ to prolong the EIT light storage time of weak coherent probe pulses. In our experiment, we set the static magnetic field to $\vec{B}_0 = (-65, 158, 385)$ G (in a coordinate system where $x \parallel D_1$, $y \parallel D_2$, and $z \parallel b$, with the crystal axes D_1, D_2, and b) which corresponds to the ZEFOZ point labeled 'B' in [45]. This is a different choice compared to our previous work [6, 46] and enables longer T_2 at a lower magnetic field [45].

Perfectly matching the magnetic field to ZEFOZ is crucial to achieve long T_2 time. Even 1% deviation from ZEFOZ conditions can lead to a reduction of T_2 by an order of magnitude [46]. In order to account for daily fluctuations of the magnetic background field in the laboratory we perform an optimization of the magnetic field for ZEFOZ based on a gradient descent search algorithm prior to all experiments [46].

We note, that under ZEFOZ conditions with the resulting complex level splittings (see figure 1), preparation of an appropriate absorption spectrum for EIT light storage in Pr:YSO is quite complicated. We use a spectral tailoring sequence [47] to generate 300 kHz wide spectral pits around ν_c and ν_p and prepare a

Table 1. Characterization of the multipass configuration under ZEFOZ conditions. Storage efficiency η_{LS}, transmission $\mathcal{T}$, and setup efficiency η vs number of passes N through the memory crystal. The storage time is $t_s = 2\ \mu$s.

N	η_{LS} (%)	$\mathcal{T}$ (%)	η (%)
1	11.3 ± 0.2	84.3 ± 0.4	9.5 ± 0.1
2	19.0 ± 0.2	72.7 ± 0.6	13.8 ± 0.2
3	23.3 ± 0.6	61.8 ± 0.5	14.4 ± 0.4

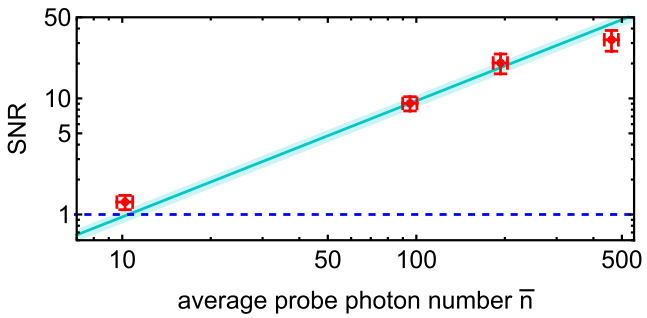

Figure 4. SNR in EIT light storage at the ZEFOZ point vs average input probe photon number $\bar{n}$. The storage time is $t_s = 2\ \mu$s. Note the logarithmic scale on both axes. We use a double pass through the memory. Red data points indicate experimental data. The turquoise, solid line represents a linear fit with standard deviation shown as a shaded area. The dashed, blue line indicates SNR = 1.

200 kHz wide absorption plateau with OD ≈ 2 centered at ν_p. The preparation of an absorption plateau slightly increases the storage efficiency compared to a single absorption peak due to a steeper dispersion. This yields a lower group velocity in EIT light storage and, hence, better conditions to stop the light pulse.

We must not fail to mention, that the level splittings under ZEFOZ conditions reduce the OD at the probe transition. This reduces the possible storage efficiency compared to the field-free case. To compensate for the lower OD, we apply our multipass setup [23]. However, while more passes N increase the EIT light storage efficiency, they also lead to higher losses at all optics in the multipass setup. The total setup efficiency η is given by the product of the light storage efficiency η_{LS} (which increases with N) and the transmission $\mathcal{T}$ of the multipass setup (which decreases with N).

We performed a systematic measurement of the variation of η with N for storage of classical pulses. For each N we optimized the magnetic field for maximal T_2. This was required, as the magnetic field setting varies slightly with the number of passes N due to field inhomogeneity and finite storage volume. Afterwards, following the approach of [41, 42], we optimized the temporal profile of the probe pulse to obtain maximal storage efficiency η_{LS} at short storage time $t_s = 2\ \mu$s. Finally, we measured the transmission $\mathcal{T}$ of the multipass setup. We show the results in table 1 for $N = 1, 2$, and 3 passes. As expected, the light storage efficiency η_{LS} grows with increasing N while the transmission $\mathcal{T}$ drops. Due to these counteracting effects, the total setup efficiency η increases only very little from $N = 2$ to $N = 3$. Furthermore, we find that T_2 drops for $N = 3$. This is due to non-perfect overlap of the beams from multiple passes and inhomogeneity of the magnetic field. Therefore, we decide to apply our setup in double pass configuration ($N = 2$) as this simplifies the alignment and reduces the effect of vibrations on the light storage experiments of weak coherent pulses at prolonged storage time.

We proceed now towards EIT light storage of few photon pulses under ZEFOZ conditions. In a first measurement we determine the SNR for light storage in our setup supported by ZEFOZ, but without DD or rephasing by RF pulses, which might cause additional signal loss and noise. We intend to compare the obtained SNR to the case without ZEFOZ. Hence, we first choose a short storage time $t_s = 2\ \mu$s. However, we now also optimize the probe pulse shape using intense pulses in the classical regime, and attenuate the pulses afterwards to the few photon level.

Figure 4 shows the measured SNR for different average photon numbers $\bar{n}$ in the probe pulse under ZEFOZ conditions at the short storage time. From a linear fit to the data (see turquoise line in figure 4) we find that for SNR = 1 we require $\bar{n} = 10.5 \pm 1.3$. Comparison to our results on single photon storage without magnetic field (see figure 3) shows that under ZEFOZ conditions we require roughly 30 times more probe photons to obtain a similar SNR. This is due to the lower storage efficiency (by a factor of two) at lower OD under ZEFOZ conditions. Moreover, in this case the induced level splittings and shifts lead to a

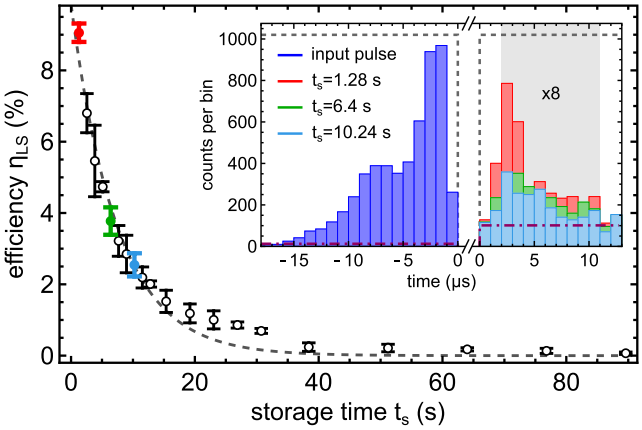

Figure 5. Light storage efficiency η_{LS} under ZEFOZ conditions and with UR64 DD sequences vs storage time t_s. We use a double pass through the memory. Data points show the experimental results for storage of classical light pulses. The dashed line is a fitted exponential decay with (7.5 ± 0.4) s decay time. Single data points set in color indicate the storage times for which we also store weak coherent pulses with $\bar{n} = 52 \pm 2$. Inset: photon counts of the input pulse (blue) and signal pulses vs time for storage times of $t_s = 1.28$ s (red), 6.4 s (green), and 10.24 s (cyan). The signal traces for the latter storage times are accumulated over 1000, 750, and 1250 repetitions, respectively. For better comparison all counts are normalized to 1000 repetitions. The dashed, gray line indicates the temporal shape of the control pulses and the dash-dotted, purple line shows the average noise level. The gray shaded area indicates the integration gate for the signal.

decreased frequency difference between probe and control $\nu_p - \nu_c = 7.3$ MHz. This causes another SNR reduction by a factor of two due to residual absorption of probe photons in the filter crystal, as we require a slightly different and less efficient preparation sequence for the filter crystal. The remaining reduction of the filter performance is caused by the reduced control suppression at this smaller frequency difference $\nu_p - \nu_c$. Nevertheless, we achieve a suppression of the control background by 110 dB even under the challenging conditions of ZEFOZ. The results show that EIT light storage of weak coherent pulses at the few photon level is also possible in combination with ZEFOZ.

3.3. Adding DD to the storage protocol

We combine now ZEFOZ with DD in order to further prolong and exploit the coherence time for EIT light storage. In the simplest approach, we may use sequences of π pulses with their frequency matched to the spin transition for rephasing during the storage time. However, π pulses are never perfect, e.g. due to fluctuations (pulse errors) in their amplitude, center frequency, or temporal shape. Hence, they will not work perfectly to rephase the spin wave. To compensate for such problems, we apply a universal robust (UR) composite rephasing sequence of RF pulses [48, 49]. The phases of the single pulses in the UR sequence serve as control parameters to drive the Bloch vector (which represents the state of the spin transition carrying the atomic coherences) on robust pathways through Hilbert space, which are less sensitive to pulse errors of the single π pulses. The error compensation capability of UR sequences increases with their order, i.e. the number of π pulses in the sequence. However, the sequence duration (and consequently its order) is limited by the coherence time of the spin transition of the individual quantum systems in the ensemble. We find that a time separation of 20 ms between the π pulses of the UR sequence and an order of 64 (defining a UR64 sequence, for short) yield the largest rephasing efficiency and coherence time in our system. For a single cycle of a UR64 sequence, i.e. at $t_s = 1.28$ s, we measure a rephasing efficiency of 45%. We found that this is a factor of 5 larger compared to a simple, conventional sequence of rephasing π pulses with equal phases (CPMG). Hence, the UR sequences outperform conventional rephasing sequences by far. Shorter time delay between the pulses should lead to even longer T_2. However, at shorter time delay the high-repetition RF pulses caused stray fields which affected the frequency stability of our laser system—which is a solvable issue for future improvements of the experiment.

Figure 5 shows the EIT light storage efficiency for classical pulses versus storage time when we apply both ZEFOZ and UR64 rephasing sequences as discussed above. A simple exponential fit (dashed line) of the data yields a coherence time $T_2 = (7.5 \pm 0.4)$ s and a storage efficiency of $\eta_{LS}^{(0)} = (9.9 \pm 0.4)\%$ at $t_s = 0$. This represents an increase of T_2 by a factor of four using DD compared to rephasing by two π pulses only.

We note, that compared to our previous work on EIT storage of classical pulses [6] T_2 is roughly a factor of six shorter now. However, in the latter work the storage efficiency was around 0.5% only—while we get two orders of magnitude higher efficiency now. In the previous work the efficiency was limited due to application of a CPMG sequence, which led to a strong variation of the storage efficiency with the phase of

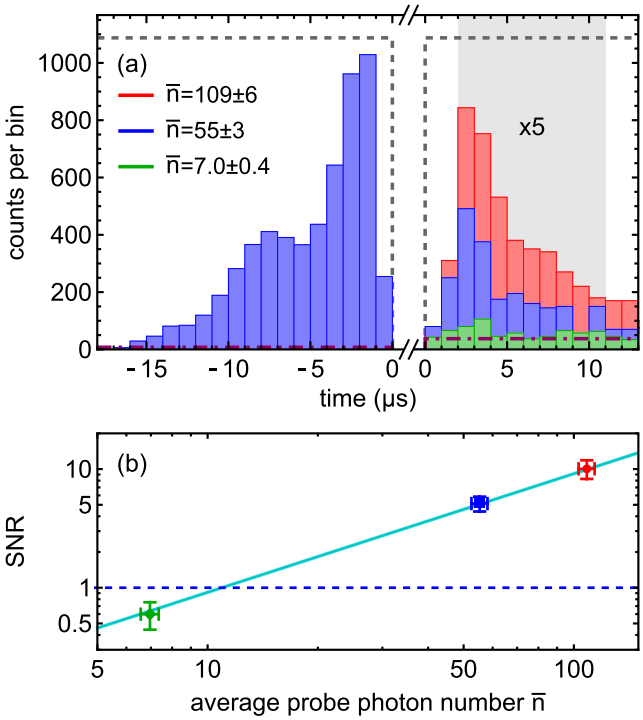

Figure 6. EIT light storage of weak coherent probe pulses under ZEFOZ conditions and with a UR64 DD sequence, at a long storage time of $t_s = 1.28$ s. (a) Photon counts of probe and signal pulses for average probe photon numbers $\bar{n} = 109 \pm 6$ (red), 55 ± 3 (blue), and 7.0 ± 0.4 (green) vs time. The counts are accumulated over 500, 1000, and 1750 repetitions, respectively, and normalized to 1000 repetitions for better comparison. In order not to overload the figure, we only show the input probe pulse shape for $\bar{n} = 55 \pm 3$. The dashed, gray line indicates the temporal shape of the control pulses and the dash-dotted, purple line shows the average noise level. The gray shaded area indicates the integration gate for the signal. (b) SNR vs average input probe photon number $\bar{n}$. Note the logarithmic scale on both axes. Data points in color depict experimental results based upon the measurements in the above figure (a). The turquoise, solid line shows a linear fit to the data. The dashed, blue line indicates SNR = 1.

the stored coherence. Since in our configuration the phase of the coherence varies strongly within the medium, a large part of the stored spin wave was lost. At the same time it enabled a very efficient rephasing of the little bit of remaining coherence. This permitted a long T_2 time at this particular phase [49]. However, such a protocol is not appropriate for applications in a quantum memory, where the storage and retrieval efficiency must be independent of the input phase. The UR sequences permit such phase-insensitive operation in a quantum memory, i.e. they work at high efficiency for arbitrary phase. Our results demonstrate one of the longest storage times for a memory ready to work on the few photon level to date. Moreover, the obtained storage efficiency is quite high compared to other optical memories (with potential as a quantum memory) operated at long storage times of 1 s or beyond [5, 6, 18–20, 50, 51].

3.4. Storage of weak coherent pulses at long times

We proceed now towards storage of weak coherent probe pulses, involving ZEFOZ, rephasing by composite UR sequences and a double pass geometry through the memory. The inset in figure 5 shows the photon counts of input probe pulses containing an average photon number $\bar{n} = 52 \pm 2$ (blue data), as well as the photon counts for the retrieved signal pulses at storage times of $t_s = 1.28$ s, 6.40 s, and 10.24 s. We can clearly distinguish the weak coherent signal pulses from the background (indicated by the dash-dotted, purple line) even for the longest storage time of $t_s = 10.24$ s. From the data we determine storage efficiencies of $\eta_{LS} = (5.6 \pm 0.4)\%$, $(3.0 \pm 0.5)\%$, and $(1.7 \pm 0.3)\%$ for $t_s = 1.28$ s, 6.4 s, and 10.24 s, respectively. Considering the integration gate this is consistent with the measurement for classical pulses (only slightly lower for the retrieved few photon pulses at $t_s = 1.28$ s). The data confirm that we maintain the coherence time of $T_2 = 7.5$ s measured for classical pulses also at the few photon level. To the best of our knowledge, our results represent the first demonstration for storing weak coherent pulses on a 10 s timescale. The coherence time of $T_2 = 7.5$ s pushes the state-of-the-art by more than an order of magnitude [8]. We note, however, that at present the background noise prevented us from storing also single photon pulses with $\bar{n} = 1$ on this very long timescale of many seconds.

We explore now the limits of our memory at a fixed storage time of $t_s = 1.28$ s. Figure 6(a) shows the photon counts for EIT storage of pulses with different average photon numbers. The retrieved signal pulses

for $\bar{n} = 109$ (red) and $\bar{n} = 55$ (blue) can easily be distinguished from the background noise. The retrieved pulse with $\bar{n} = 7$ (green) is just visible above the noise level. The SNR in this case is 0.6 ± 0.2. Hence, we can still get a well detectable signal for EIT storage of a few photon pulse with $\bar{n} = 7$ for a long storage time above 1 s. When we determine and plot the SNR for the three pulses at different photon numbers (see figure 6(b)), we can estimate by a linear fit (turquoise line) the input probe pulse photon number required to obtain an SNR of 1 (dashed, blue line). From the fit we see that this is the case for an input probe pulse with roughly 10 photons which corresponds to a noise floor of 0.062 photons per experimental trial.

To analyze the source of the residual noise, we prepare the memory crystal transparent (over a spectral range of 10.5 MHz) and then apply a control pulse which is detuned by 3.7 MHz, i.e. twenty times its Rabi frequency, from the closest populated transition. Therefore, we do not expect effects other than surface reflections to contribute to the noise floor. Here, we find a noise floor of 0.051 photons per trial, which is close to the value obtained in the light storage experiments. From this we conclude that the main contribution to the noise is indeed due to surface reflections (leaking through the filter, as discussed above) and other effects such as, e.g. Raman scattering, seem to be negligible.

Our light storage data show that at the single photon level we get SNR $= 0.091 \pm 0.002$. Though this is not yet sufficient for single photon storage, the data nevertheless confirm EIT light storage at the few photon level, beyond 1 s storage time, implemented in a solid-state system. The findings are of relevance also to other protocols in such media.

4. Summary and conclusion

We experimentally demonstrated light storage towards the single photon level at a long storage time of several seconds by EIT in a Pr:YSO memory crystal. We applied decoherence control by precisely controlled static magnetic fields in three dimensions to prepare the medium at ZEFOZ conditions and universal robust composite RF pulse sequences for efficient dynamical decoupling. This pushed the coherence and storage times towards the regime of seconds. As an important feature for a memory ready to work at the quantum limit, the composite sequences permit constant rephasing efficiency for arbitrary input phase. We used a simple ring-type multipass setup around the memory crystal to improve the optical depth and storage efficiency. This is important in particular under ZEFOZ conditions when the complex level splittings reduce the available optical depth. To separate the signal at the level of few or single photons from optical background, which is mainly induced by intense control pulses, we used a Pr:YSO filter crystal prepared by appropriate optical pumping sequences. We implemented a multipass setup also around the filter crystal to improve the optical depth and spectral selectivity. Such, we achieved a suppression of optical noise by 110 dB, which enabled operation of the memory at the level of weak coherent pulses. The multipass filter setup is adaptable to the specific requirements of the storage process, e.g. also to other storage protocols. In contrast to related previous work [52–55], the suppression level is easily controllable by the number of passes.

Already without decoherence control, our setup permitted storage of weak coherent pulses with an average photon number $\bar{n} = 1.1$ at a storage time of 2 μs and a storage efficiency of 42%. This exhibits the first implementation of EIT light storage at the single photon level in a solid-state system. Proceeding even further with decoherence control by ZEFOZ and dynamical decoupling we demonstrated storage of weak coherent pulses containing some 10 photons up to the time scale of 10 s. At a storage time of $t_s = 1.28$ s, we achieved a storage efficiency of $\eta_{LS} = (5.6 \pm 0.4)\%$ for weak coherent pulses. We still get a well detectable signal for EIT light storage of a few photon pulse with an average photon number $\bar{n} = 7$ for this long storage time exceeding 1 s. We found the residual background noise to be roughly an order of magnitude too large to permit storage of a pulse with $\bar{n} = 1$ at the long time scale beyond 1 s. In future improvements of our setup, we will pre-filter the control beam and reduce the laser linewidth. This should further reduce the noise level by the required amount to also enable storage of a single photon for long times and allow us to proceed towards qubit storage. Nevertheless, our experimental demonstrations for storage of few photon light pulses at long times in a solid-state memory as presented in this paper set a new benchmark for light storage, irrespective of the storage protocol or medium.

Data availability statement

The data that support the findings of this study are available upon reasonable request from the authors.

ORCID iDs

Marcel Hain https://orcid.org/0000-0001-8213-0797
Markus Stabel https://orcid.org/0000-0003-3837-641X
Thomas Halfmann https://orcid.org/0000-0002-1222-2669

References

[1] Briegel H-J, Dür W, Cirac J I and Zoller P 1998 *Phys. Rev. Lett.* **81** 5932
[2] Simon C *et al* 2010 *Eur. Phys. J.* D **58** 1
[3] Cho Y-W *et al* 2016 *Optica* **3** 100
[4] Hsiao Y-F *et al* 2018 *Phys. Rev. Lett.* **120** 183602
[5] Ma Y, Ma Y-Z, Zhou Z-Q, Li C-F and Guo G-C 2021 *Nat. Commun.* **12** 2381
[6] Heinze G, Hubrich C and Halfmann T 2013 *Phys. Rev. Lett.* **111** 033601
[7] Wang Y, Li J, Zhang S, Su K, Zhou Y, Liao K, Du S, Yan H and Zhu S-L 2019 *Nat. Photon.* **13** 346
[8] Körber M, Morin O, Langenfeld S, Neuzner A, Ritter S and Rempe G 2018 *Nat. Photon.* **12** 18
[9] Fleischhauer M, Imamoglu A and Marangos J P 2005 *Rev. Mod. Phys.* **77** 633
[10] Heshami K, England D G, Humphreys P C, Bustard P J, Acosta V M, Nunn J and Sussman B J 2016 *J. Mod. Opt.* **63** 2005
[11] Afzelius M, Simon C, de Riedmatten H and Gisin N 2009 *Phys. Rev.* A **79** 052329
[12] Alexander A L, Longdell J J, Sellars M J and Manson N B 2006 *Phys. Rev. Lett.* **96** 043602
[13] Kraus B, Tittel W, Gisin N, Nilsson M, Kröll S and Cirac J I 2006 *Phys. Rev.* A **73** 020302(R)
[14] Ma Y-Z, Jin M, Chen D-L, Zhou Z-Q, Li C-F and Guo G-C 2021 *Nat. Commun.* **12** 4378
[15] Nunn J, Reim K, Lee K C, Lorenz V O, Sussman B J, Walmsley I A and Jaksch D 2008 *Phys. Rev. Lett.* **101** 260502
[16] Gorshkov A V, André A, Lukin M D and Sørensen A S 2007 *Phys. Rev.* A **76** 033805
[17] Schnorrberger U, Thompson J D, Trotzky S, Pugatch R, Davidson N, Kuhr S and Bloch I 2009 *Phys. Rev. Lett.* **103** 033003
[18] Zhang R, Garner S R and Hau L V 2009 *Phys. Rev. Lett.* **103** 233602
[19] Dudin Y O, Li L and Kuzmich A 2013 *Phys. Rev.* A **87** 031801(R)
[20] Katz O and Firstenberg O 2018 *Nat. Commun.* **9** 2074
[21] de Riedmatten H and Afzelius M 2015 Quantum Light Storage in Solid State Atomic Ensembles *Engineering the Atom-Photon Interaction* ed A Predojević and M Mitchell (Heidelberg: Springer) pp 241–273
[22] Zhong T and Goldner P 2019 *Nanophotonics* **8** 2003
[23] Schraft D, Hain M, Lorenz N and Halfmann T 2016 *Phys. Rev. Lett.* **116** 073602
[24] Afzelius M and Simon C 2010 *Phys. Rev.* A **82** 022310
[25] Moiseev S A, Andrianov S N and Gubaidullin F F 2010 *Phys. Rev.* A **82** 022311
[26] Jobez P, Usmani I, Timoney N, Laplane C, Gisin N and Afzelius M 2014 *New J. Phys.* **16** 083005
[27] Sabooni M, Li Q, Kröll S and Rippe L 2013 *Phys. Rev. Lett.* **110** 133604
[28] Akhmedzhanov R A, Gushchin L A, Kalachev A A, Nizov N A, Nizov V A, Sobgayda D A and Zelensky I V 2016 *Laser Phys. Lett.* **13** 115203
[29] Davidson J H, Lefebvre P, Zhang J, Oblak D and Tittel W 2020 *Phys. Rev.* A **101** 042333
[30] Beil F, Klein J, Nikoghosyan G and Halfmann T 2008 *J. Phys. B: At. Mol. Opt. Phys.* **41** 074001
[31] Nilsson M, Rippe L, Kröll S, Klieber R and Suter D 2004 *Phys. Rev.* B **70** 214116
[32] Fraval E, Sellars M J and Longdell J J 2004 *Phys. Rev. Lett.* **92** 077601
[33] Viola L, Knill E and Lloyd S 1999 *Phys. Rev. Lett.* **82** 2417
[34] Mieth S, Henderson A and Halfmann T 2014 *Opt. Express* **22** 011182
[35] Wen Y, Zhou P, Xu Z, Yuan L, Wang M, Wang S, Chen L and Wang H 2020 *Opt. Express* **28** 360
[36] Ma L, Slattery O and Tang X 2017 *J. Opt.* **19** 043001
[37] Ma L, Slattery O and Tang X 2018 *Mod. Phys. Lett.* B **32** 1830001
[38] Beavan S E, Goldschmidt E A and Sellars M J 2013 *J. Opt. Soc. Am.* B **30** 1173
[39] Kinos A, Li Q, Rippe L and Kröll S 2016 *Appl. Opt.* **55** 10442
[40] Sabooni M, Nilsson A N, Kristensson G and Rippe L 2016 *Phys. Rev.* A **93** 013842
[41] Gorshkov A V, André A, Fleischhauer M, Sørensen A S and Lukin M D 2007 *Phys. Rev. Lett.* **98** 123601
[42] Novikova I, Gorshkov A V, Phillips D F, Sørensen A S, Lukin M D and Walsworth R L 2007 *Phys. Rev. Lett.* **98** 243602
[43] Carr H Y and Purcell E M 1954 *Phys. Rev.* **94** 630
[44] Meiboom S and Gill D 1958 *Rev. Sci. Instrum.* **29** 688
[45] Longdell J J, Alexander A L and Sellars M J 2006 *Phys. Rev.* B **74** 195101
[46] Heinze G, Hubrich C and Halfmann T 2014 *Phys. Rev.* A **89** 053825
[47] Lauritzen B, Timoney N, Gisin N, Afzelius M, de Riedmatten H, Sun Y, Macfarlane R M and Cone R L 2012 *Phys. Rev.* B **85** 115111
[48] Genov G T, Schraft D, Vitanov N V and Halfmann T 2017 *Phys. Rev. Lett.* **118** 133202
[49] Genov G T, Schraft D and Halfmann T 2018 *Phys. Rev.* A **98** 063836
[50] Longdell J J, Fraval E, Sellars M J and Manson N B 2005 *Phys. Rev. Lett.* **95** 063601
[51] Holzäpfel A, Etesse J, Kaczmarek K T, Tiranov A, Gisin N and Afzelius M 2020 *New J. Phys.* **22** 063009
[52] Beavan S E, Hedges M P and Sellars M J 2012 *Phys. Rev. Lett.* **109** 093603
[53] Gündoğan M, Ledingham P M, Kutluer K, Mazzera M and de Riedmatten H 2015 *Phys. Rev. Lett.* **114** 230501
[54] Seri A, Lenhard A, Rieländer D, Gündoğan M, Ledingham P M, Mazzera M and de Riedmatten H 2017 *Phys. Rev.* X **7** 021028
[55] Yang T-S *et al* 2018 *Nat. Commun.* **9** 3407